OPEN ACCESS
IOP Publishing | Songshan Lake Materials Laboratory
Materials Futures
Mater. Futures **2** (2023) 025002 (8pp)
https://doi.org/10.1088/2752-5724/acbd63

Combinatorial development of antibacterial FeCoCr-Ag medium entropy alloy

Jiashu Cao[1,2,6], Xin Jiang[3,6], Qinghua Zhang[1], Fusen Yuan[1], Jihao Yu[1], Fan Yang[1], Mingxing Li[1], Chao Wang[1], Ying Lu[1,3], Ming Li[1,3], Weihua Wang[1,2,3,5] and Yanhui Liu[1,3,4,5,*]

[1] Institute of Physics, Chinese Academy of Sciences, Beijing 100190, People's Republic of China
[2] School of Physical Science, University of Chinese Academy of Sciences, Beijing 100049, People's Republic of China
[3] Songshan Lake Materials Laboratory, Guangdong 523808, People's Republic of China
[4] Center of Materials Science and Optoelectronics Engineering, University of Chinese Academy of Sciences, Beijing 100049, People's Republic of China
[5] Beijing Advanced Innovation Center for Materials Genome Engineering, Beijing 100083, People's Republic of China

E-mail: yanhui.liu@iphy.ac.cn

Received 30 December 2022, revised 9 February 2023
Accepted for publication 16 February 2023
Published 20 March 2023

Abstract

Antibacterial activity and mechanical properties of FeCoCr-Ag medium entropy alloys were studied via combinatorial fabrication paired with high-throughput characterizations. It was found that the antibacterial activity and mechanical properties exhibit non-linear dependence on the content of Ag addition. Within the studied alloys, $(FeCoCr)_{80}Ag_{20}$ possesses an optimized combination of different properties for potential applications as antibacterial coating materials. The underlying mechanism is ascribed to the formation of a dual-phase structure that leads to competition between the role of Ag phase and FeCoCr phase at different Ag content. The results not only demonstrate the power and effectiveness of combinatorial methods in multi-parameter optimization but also indicate the potential of high entropy alloys as antibacterial materials.

Keywords: antibacterial metals and alloys, medium entropy alloy, combinatorial method

[6] These authors contributed equally to this work.
[*] Author to whom any correspondence should be addressed.

Future perspectives
Compositionally complex alloys provide a vast compositional space for the development of potential antibacterial coating materials. To meet the requirements in practical applications, antibacterial materials need to integrate a variety of properties, such as strength, processability, adhesion to substrate, antibacterial activity, etc. However, alloy development has heavily relied on sequential trial-and-error methods. There methods are often time consuming and labor intensive. Combinatorial method offers an ideal solution to overcome these problems. In contrast to conventional alloy development, combinatorial fabrications paired with high-throughput characterizations facilitate parallel preparation and steering through a wide range of compositions. These allow effective establishment of the composition-property relationship and reveal the compositional dependence of these properties. Based on the combinatorial approach, functional materials that satisfy required combination of optimized properties could be discovered more efficiently.

1. Introduction

Bacterial infections upon contact have invoked continued efforts in the development of antibacterial coatings, which are required in broad areas ranging from public transportation to medical devices. To meet the requirements in practical applications, an antibacterial coating material needs to integrate a variety of properties [1, 2], such as strength, processability, adhesion to substrate, antibacterial activity, etc. Recently, high-entropy alloys have attracted increasing attention due to their remarkable mechanical properties [1, 2], corrosion resistance [3], processability [4, 5], etc. Although many of these attributes are desired for antibacterial coating materials, the development of antibacterial high-entropy alloys has received less attention until recently [6–8].

The antibacterial activity of the current high-entropy alloys has been attributed to membrane damage [9], oxidative stress [7] and protein denaturation, all of which are induced by Cu, one of the main constituent elements in many high-entropy alloys. Compared with Cu, Ag has long been known to be more effective in killing a wider range of bacteria and microbials [10–14]. In particular, Ag has often been added as an alloying element in a variety of implanted materials to form antibacterial alloys. To achieve a balanced combination of properties, the amount of Ag addition needs to be optimized. However, high-entropy alloys are usually composed of more than three elements. With sequential trial-and-error methods, it is a daunting task to identify the optimal Ag addition that results in combined properties, not to mention that most alloy development methods are devised to screen individual properties.

In this study, we report on the combinatorial optimization of Ag addition in an FeCoCr system. We select this alloy system because the FeCoCr alloy system was reported to be an efficient coating of carbon steel in an aggressive marine environment due to its high corrosion resistance [15]. In addition, Co-Cr can greatly enhance the toughness, hardness and wear resistance [16]. In addition to antibacterial activity, we also evaluated the variation of hardness, and adhesion to a substrate, with the addition of Ag. We identify an optimal amount of Ag addition that combines antibacterial activity, hardness, and adhesion to stainless-steel substrate.

2. Materials and methods

Combinatorial thin films of FeCoCr-Ag were deposited by using magnetron co-sputtering on Si (100) wafers with a diameter of 4 inches. The base pressure of the chamber was 8.0×10^{-5} Pa. Ar gas (purity $>$ 99.999 vol.%) was introduced into the sputtering chamber to maintain an equilibrium chamber pressure of 1.0 Pa during the film deposition process. Pure Ag (purity $>$ 99.99 wt.%) and FeCoCr alloy (Fe:Co:Cr $=$ 1:1:1; purity $>$ 99.9 wt.%) targets were used for the sputtering at room temperature. The variation of Ag content was controlled by the tilt of the sputtering gun and sputtering power. The combinatorial films have a thickness of $\sim$1 μm. Chemical analyses of the combinatorial films were performed using scanning electron microscopy (SEM) equipped with an energy-dispersive x-ray spectroscopy detector (Phenom XL). X-ray diffraction (XRD) was used to characterize the structure of the films (PANalytical EMPYREAN diffractometer with Cu-Kα radiation and an automated XY-stage). Glance-incidence XRD (GI-XRD) was conducted on a Bruker D8 diffractometer. Phase formation and microstructure of the FeCoCr-Ag thin films were further characterized using an ARM200F scanning transmission electron microscope (STEM). A high-angle annular dark field (HAADF) detector was used for the imaging in mass-thickness contrast mode. The specimens for STEM analysis of the films were prepared with a focused ion beam and SEM (Helios 600i).

The combinatorial film was covered by a custom-made acrylic 80-well plate that is compatible with the standard 96-well plate. This not only allows isolation of different alloys from each other but also parallel evaluation of antibacterial activity in up to 80 alloys. The samples and the acrylic well plates were sterilized in ethanol for 30 min followed by rinsing with distilled water and drying. The bacterial strain of Gram-negative *Escherichia coli* (K-12, MG1655 Strain) was cultured at 37 °C for 8–10 h in Luria-Bertani (LB) agar broth (10 g l^{-1} tryptone, 5 g l^{-1} yeast extract, 10 g l^{-1} NaCl and 25 g l^{-1} agar). The monoclone was activated and transferred to LB liquid broth for 2 h expansion culture. Diluted broth with a bacterial number density of 1×10^8 ml^{-1} was used for antibacterial activity evaluation. About 250 μl of bacterial growth medium was applied to the surface of each alloy and cultured in an incubator at 37 °C. Optical density (OD) values at a wavelength of 600 nm (OD600) were measured by a microplate reader (Epoch, BioTek) at incubation times of 1, 3, 6 and 12 h, respectively. For positive control, bacteria with LB broth were incubated on a bare Si wafer. For negative control, blank LB broth without any bacteria was incubated in the samples. The bacterial growth medium in the FeCoCr-Ag alloy was diluted 1000 times by phosphate buffered saline (PBS: 1.44 g/L Na2HPO4, 0.24 g/L KH2PO4, 8 g/L NaCl, pH 7.4) and stained by SYTO9 and propidium iodide (LIVE/DEAD®

BacLight Bacterial Viability Kit, Life Technologies, Thermo Fisher). After 15 min of dark incubation at room temperature, the stained bacterial suspension was observed by structured illumination microscopy (Ti2 fluorescence microscopy, Nikon). SYTO9 was excited by a 488 nm laser, and propidium iodide was excited by a 561 nm laser. The number of live and dead cells was analyzed using ImageJ software.

Hardness (H) and Young's modulus (E) were measured by using nanoindentation (Bruker TI 980 TriboIndenter instrument). For all tests, the peak load was set at 4500 μN with the indent depth at about 100 nm. The tests were performed with a 5 s loading time, 2 s holding time and 5 s unloading time. The water contact angle was measured via a Dataphysics OCA20 contact angle system, and 4 μl of deionized water was used for each test. Adhesion tests were performed on films containing 7, 20, 30, 40, 50 and 60 at.% Ag, which was deposited on 304 stainless-steel disks on a mirror-polished surface. The diameter of the 304 stainless-steel disk is 20 mm. Semi-transparent pressure-sensitive tape of 3M600 standard adhesion strength was applied to the thin films. After 1 min, the tape was peeled off by seizing the free end and pulling it at an angle of 90°. The surface morphologies of the films were observed using an MFP-3D-SA standard atomic force microscope (AFM) in AC mode. A Tap 300 Al-G probe with a resonant frequency of 300 kHz and a force constant of 40 N m^{-1} was used.

3. Results

3.1. Materials library and compositional gradient

An alloy library with gradient composition can be obtained through magnetron co-sputtering [17]. In contrast to other co-sputtering with pure metal targets, we used equal atomic FeCoCr alloy and pure Ag as targets (figure 1(a)). The co-sputtering results in a combinatorial alloy library with increasing Ag content, while the ratio of Fe, Co and Cr is maintained constant (Fe:Co:Cr = 1:1:1). This not only enables us to effectively identify the optimal Ag content but also elucidates the effect of Ag addition on antibacterial activity. Figure 1(b) presents the compositional range covered by our combinatorial alloy libraries. A broad range of Ag content ranging from 4–80 at.% is included in the libraries.

The addition of Ag induces gradual changes in phase formation (figure 1(c)). The XRD pattern reveals that the film with Ag less than 15 at.% is mainly composed of a tetragonal phase (TP) with a space group of P42 mnm^{-1} (136)(PDF#05-0708) and cubic phase with a space group of $I\bar{4}3m$ (217) (PDF#51-0740). The weak diffraction peak of Ag (111) (PDF#04-0783) suggests a duplex-phase microstructure. The location of diffraction peaks in TPs remains unshifted along with increasing Ag content, suggesting that the Ag was not further embedded in the FeCoCr lattice [18]. With further increase in Ag content, the intensity of the Ag (111) peak becomes stronger than that of the FeCoCr phase, suggesting increasing formation of Ag phase. It is also worth noting that only a few diffraction peaks can be detected in the XRD patterns. This may be related to the texture of the films during deposition due to surface energy minimization [19].

STEM-HAADF images with Ag content at 7%, 20% and 70% are shown in figure 1(d). Calibration results of the FFT patterns from the TP grain boundaries prove to be Ag with face-centered cubic structure (fcc-Ag). STEM-HAADF images can reflect atomic number by bright contrast of images. This contrast indicates that the bright grain boundary phase is an Ag-rich phase, while the dark grain interior is rich in FeCoCr. This is also confirmed by interplanar spacing measurements. The interplanar spacing of the grain boundary phase is 0.23 nm, which is identical to the (111) plane of fcc-Ag, while the interplanar spacing of the grain interior is 0.20 nm, which is close to the (330) plane of TPs. Combining the corresponding FFT patterns in different areas further confirms the coexistence of TP and fcc-Ag.

It can be seen from figure 1(d) that at low Ag content (7 at.%), the films are observed to consist of a mixture of particles 15 nm in diameter and a grain boundary 1–2 nm in thickness. Further increase in Ag content (i.e. 20 at.%) results in a size decrease in the TP phase to about 7 nm and a thickness increase in the Ag-rich phase to about 5 nm. However, when the content of Ag is high (60 at.%), the thickness of the Ag-rich phase remains essentially unchanged (∼5 nm), while the size of the TP phase decreases to be less than 5 nm (figure 1(d)). This indicates that there is a critical Ag content above which an increase in the volume fraction of the Ag-rich phase is realized by forming a random network of denser grids.

3.2. Antibacterial activity assessment of FeCoCr-Ag alloy by high-throughput strategy

To evaluate in parallel the antibacterial activity of the FeCoCr-Ag alloys as a function of Ag content, we fabricated an acrylic 80-well plate with a well diameter of 5 mm and a height of 18 mm (figure 2(a)). The well spacing is designed so that the plate is compatible with both our combinatorial alloy library and automated liquid handling systems for commercial 96-well plates. The acrylic 80-well plate was attached to the combinatorial FeCoCr-Ag alloy library so that the antibacterial activity of each alloy underneath the wells can be independently assessed. We evaluate bacterial growth on alloy surfaces by measuring the optical density (OD) of the culture medium as a function of time, which is widely used for the study of bacterial growth. An increase in OD suggests an increase in bacterial concentration in the culture medium, and the alloy exhibiting the smallest OD value can be considered as the one with the best antibacterial activity within the combinatorial alloy library.

The OD600 value was measured at culture times of 1, 3, 6 and 12 h, respectively. Figure 2(b) shows an example of the contour plots displaying compositional dependent OD600 values for a culturing time of 1 h. It can be seen that the OD600 value exhibits obvious dependence on Ag content, indicating a strong correlation of antibacterial ability with the amount of Ag addition. Compared with the positive control (blank Si in this case), all here-studied FeCoCr-Ag alloys exhibit

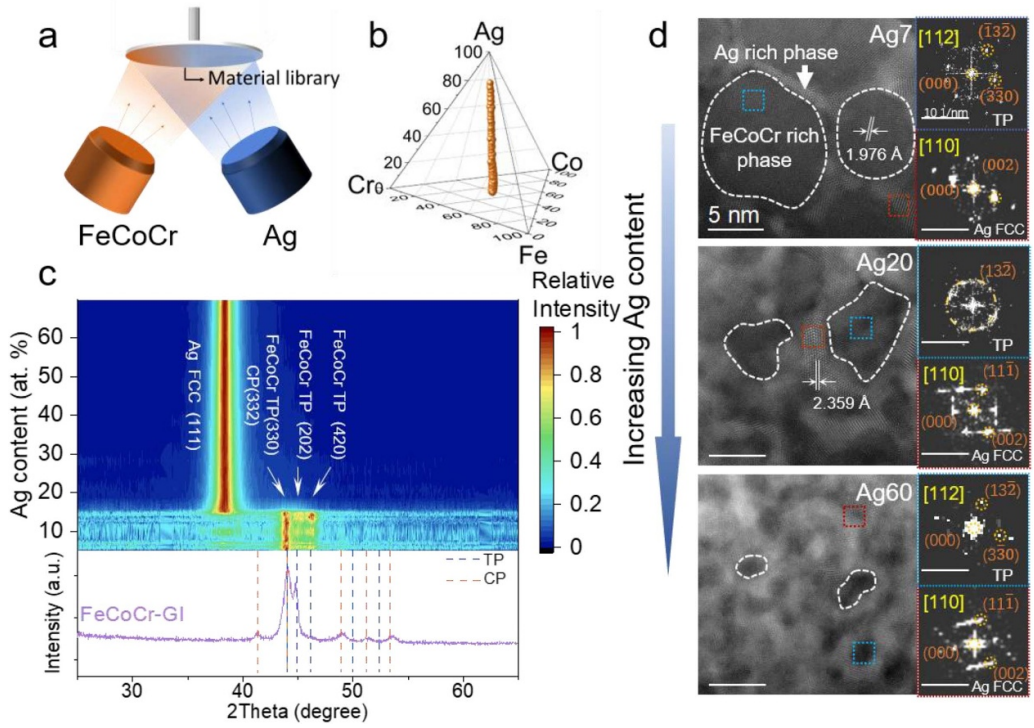

Figure 1. (a) Schematic diagram showing the co-sputtering deposition. FeCoCr-Ag alloy library is obtained by sputtering from the Ag target (blue) and FeCoCr target (orange). (b) Tetrahedral diagram of the concentration in the materials library. (c) Structural evolution with Ag content within the FeCoCr-Ag alloy library characterized by XRD and GI-XRD pattern of FeCoCr film without Ag. (d) Top-view STEM-HAADF images and corresponding fast Fourier transform (FFT) image in different areas of thin films with Ag content at 7, 20 and 60 at.%.

a significant decrease in bacterial density. For example, the OD600 value of the worst alloy within the combinatorial alloy library is still one-third lower than that of the positive control on which bacteria can freely multiply. This demonstrates the effectiveness of Ag addition in endowing antibacterial activity of FeCoCr medium alloys.

However, the dependence of antibacterial activity on Ag addition is not monolithic. Figure 2(c) summarizes the variation of OD600 as a function of Ag content for an incubation time of 12 h. A dramatic decrease in OD600 value with increasing Ag content can be observed when Ag concentration is below 20 at.%. With the further addition of Ag, a significant decrease in OD600 value is absent, suggesting the decoupling of antibacterial activity and Ag content. The results indicate that there exists an optimal Ag addition to achieve the best antibacterial activity in the FeCoCr-Ag alloy system.

The variation of OD600 value as a function of incubation time for some representative Ag additions is presented in figure 2(d), which allows the comparison of bacterial multiplication on different alloys. For all the alloys in the combinatorial alloy library, the OD600 versus time curves appear to be similar. A gradual increase in OD600 value, reflecting an increase in bacterial concentration, can be seen from a short to long incubation time. It can be seen that an increase in Ag addition results in decreased bacterial multiplication when the concentration is below 20 at.%. However, a higher amount of Ag addition does not lead to further antibacterial activity, as reflected by the nearly overlapping OD600 versus time curves for Ag addition larger than 20 at.%. The results demonstrate the effectiveness of our characterization methods in revealing the optimal Ag addition even at short incubation times.

To demonstrate the effectiveness of antibacterial activity of FeCoCr-Ag alloys as coating materials, we compare bacterial viability on surfaces of stainless steel and FeCoCr-Ag alloy with optimal Ag addition (20 at.%). The comparison was done by conducting a LIVE/DEAD analysis based on fluorescent microscopic images. As shown in figures 3(a) and (c), the number of active bacteria is similar on the two surfaces at the beginning. After 1 h of incubation, dead bacteria can be observed on the surface of the FeCoCr-20%Ag alloy (figure 3(a)), and the number of dead bacteria increases with the increase in incubation time. In contrast, few dead bacteria can be seen on the surface of 304 stainless steel after 1 h of incubation (figure 3(c)). Although several dead bacteria were seen after 6 h of incubation, the number of alive bacteria becomes obviously larger, suggesting multiplication of bacteria on 304 stainless steel. To quantitatively compare the efficiency of the FeCoCr-Ag alloy to kill bacteria, histogram plots showing the number of alive and dead bacteria are presented in figures 3(b) and (d). As can be seen, almost half of the bacteria on the FeCoCr-20%Ag alloy were dead after 1 h incubation, while the bacteria on 304 stainless steel remained active. After 6 h incubation, the number of dead bacteria on the FeCoCr-20%Ag alloy substantially increased. However, the

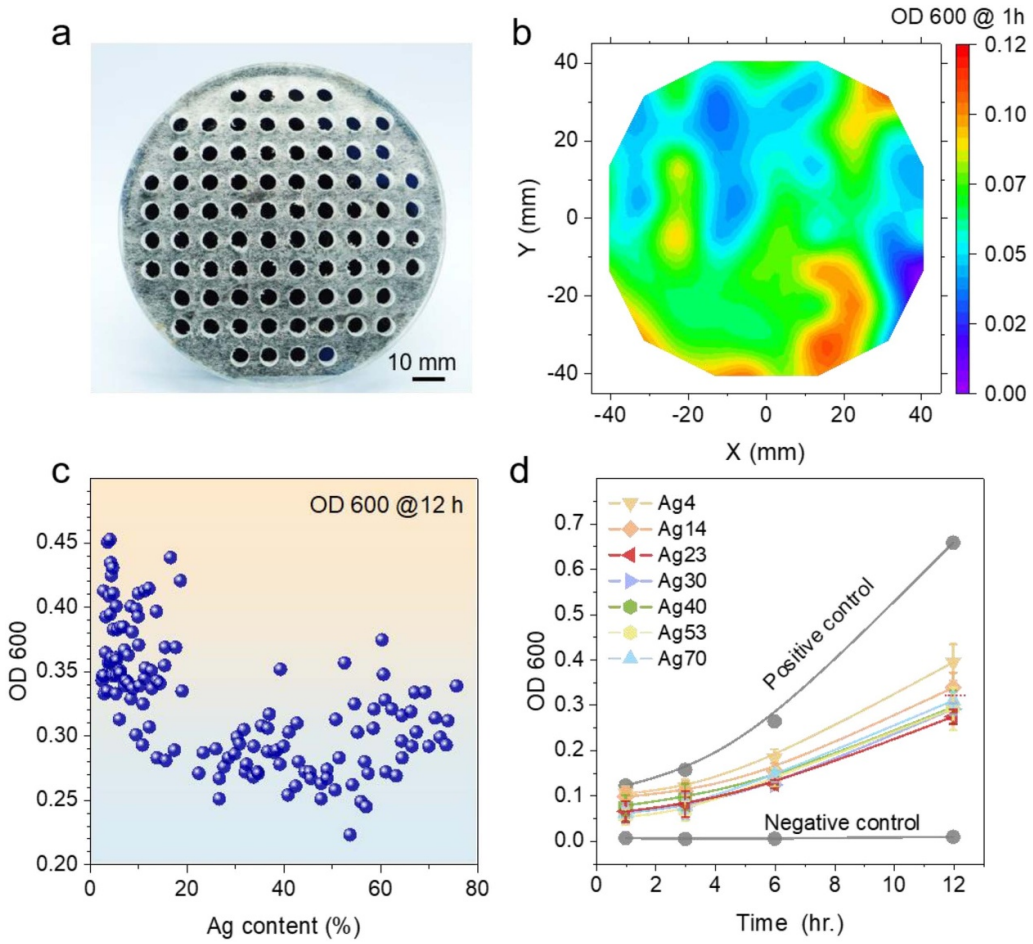

Figure 2. (a) Appearance of a materials library for antibacterial activity measurement via the high-throughput method. (b) Contour plot showing the variation of OD600 values within an alloy library at a culture time of 1 h. (c) Variation of OD600 values with Ag content for a culture time of 12 h. (d) Typical OD600 versus time curve for different Ag content. In the plots, OD600 is the OD at a wavelength of 600 nm.

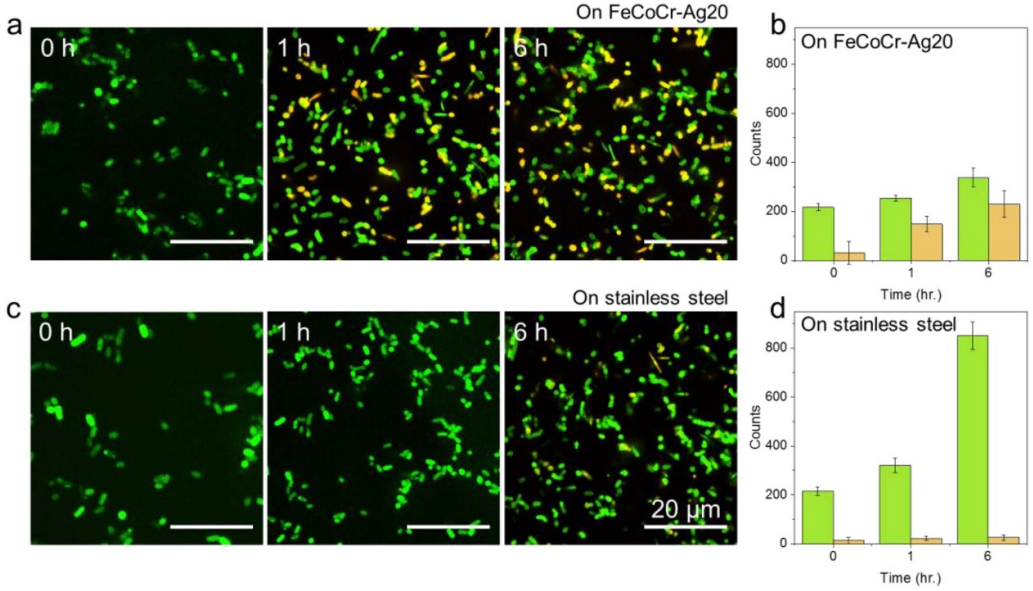

Figure 3. Comparison of antibacterial property between FeCoCr-Ag20 and 304 stainless steel. Fluorescent microscopic images of *E. coli* on FeCoCr-Ag-coated surface (a) and stainless steel surface (c) after LIVE/DEAD staining after 0 , 1 and 6 h. Scale bars in (a) and (c) are 20 μm. Counts of live (green) and dead (orange) bacteria with time on FeCoCr-Ag-coated surfaces and stainless-steel substrate are shown in (b) and (d), respectively.

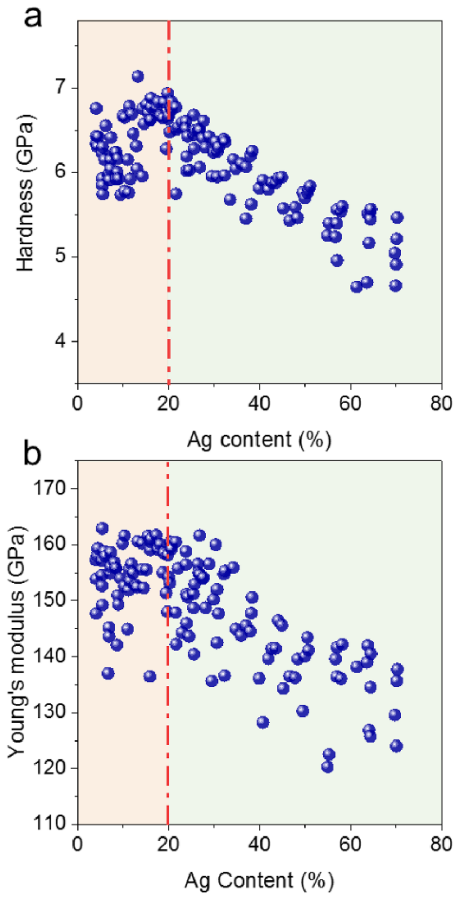

Figure 4. Variation of hardness (a) and Young's modulus (b) of the FeCoCr-Ag alloys with Ag content.

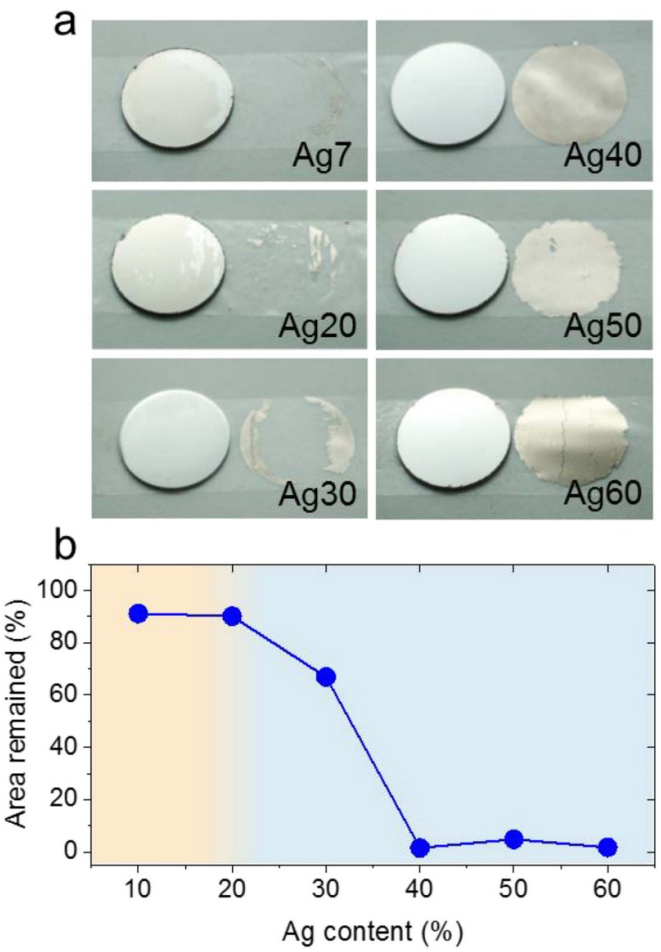

Figure 5. (a) Appearance of FeCoCr-Ag films deposited on 304 stainless-steel disks after sticking-and-pulling tests by adhesive tape. Diameter of the 304 stainless-steel disk is 20 mm. (b) Area of film that remains on 304 stainless-steel disks after the sticking-and-pulling tests.

number of dead bacteria on 304 stainless steel is very limited. The results indicate that the FeCoCr-20%Ag alloy can efficiently inhibit bacterial viability and growth and is a promising candidate as a coating material.

3.3. Mechanical property characterization of FeCoCr-Ag alloys

Unlike conventional sequential screening, the combinatorial approach allows parallel characterizations of different properties so that one can rapidly identify the alloys with optimal combination of properties. To demonstrate this, we measure hardness and elastic modulus in combinatorial materials libraries with the same compositional spread as that for antibacterial activity. The measurements were carried out using nanoindentation. Figures 4(a) and (b) show the variation of hardness and Young's modulus as a function of Ag content. One can see that the addition of Ag results in a non-monotonic change of hardness and modulus. When the content of Ag is below 20 at.%, the hardness and Young's modulus increase from 6 and 140 GPa to 7 and 160 GPa, respectively. However, further increase in the concentration of Ag leads to a decrease in hardness and modulus. When the Ag content is 70 at.%, the hardness and modulus are only 4.5 and 120 GPa, respectively. It is interesting to note that the highest hardness and modulus within the combinatorial materials library occurs at Ag concentration of 20 at.%, which coincides with that of the best antibacterial activity. This suggests that the FeCoCr-20Ag alloy as an antibacterial coating is also promising in terms of durability due to its high hardness.

3.4. Adhesion strength of FeCoCr-Ag alloys

In addition to hardness that is associated with the durability of coating, adhesion to substrate is also of concern to prevent undesired failure, in particular, peeling-off. As a rapid method to evaluate the adhesive strength, we adopt the tape sticking-and-pulling test. We deposit films on 304 stainless-steel disks on a mirror-polished surface. Adhesive tape was stuck onto the films and pulled. With this method, the entire film can be removed easily if the interface is weak. Our tests indicate that adhesive strength of the films is strongly dependent on chemical composition. As shown in figure 5, only a small fraction of the film can be removed from the 304 stainless steel when the Ag amount is below 20 at.%. For example, the area fraction of films that remain on the substrate is about 90% for Ag content of 7 at.% and 20 at.% (figure 5(b)). When

the Ag content increases to 30 at.%, a quarter of the coating can be removed and the film detaches from the substrate both at the boundary and the center of the disk. A further increase in Ag content to 40 at.% results in significantly more severe film removal. As can be seen from figure 5(a), the films can be entirely removed from the substrate at high content of Ag, indicating their weak adhesion to 304 stainless steel. Although the tape sticking-and-pulling test is a qualitative method for the evaluation of adhesive strength, the results suggest that 20 at.% the addition of Ag is optimal when considering the variation of antibacterial activity and hardness.

4. Discussion

It is well known that antibacterial activity of an alloy can be affected by either surface structure or release of metal ions. In order to reveal the dominant factor governing the variation of antibacterial activity within the combinatorial materials library, we characterized the surface morphology of the films via AFM. As shown in figure 6(a), the surface of the films is rather smooth, as indicated by the small value of roughness, and the variation of surface roughness with Ag content can be ignored. Figure 6(b) presents the surface profile of representative films. As can be seen, FeCoCr-Ag alloys possess similar domain sizes and peak-to-valley roughness, suggesting that surface structure may not be the dominant factor leading to the variation of antibacterial activity. This argument is supported by water contact angle measurements. It has been reported that bacterial adhesion is related to surface wettability. If the observed variation of antibacterial activity is controlled by the surface structure, one would expect an obvious change of contact angle with the change of Ag content. Nonetheless, this is not the case. As shown in figure 6(c), significant variation of contact angle is absent within a wide range of Ag content. Instead, the contact angle remains constant at $\sim$100° for all here-studied FeCoCr-Ag alloys. This suggests that the influence of surface structure on bacterial adhesion can be ignored, and the obvious variation of antibacterial activity can be attributed to the change of Ag content [20].

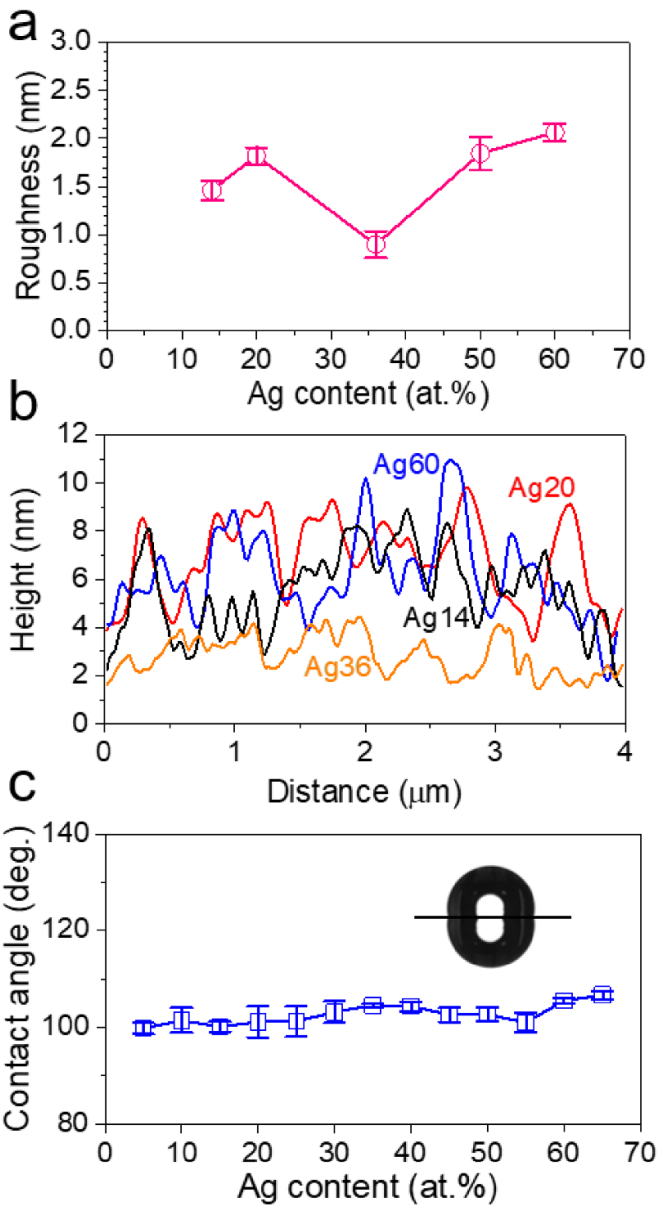

Figure 6. Surface roughness (a) and surface profile (b) for FeCoCr-Ag alloys of different Ag content. (c) Variation of water contact angle with Ag content.

It is well known that the release of metal ions is affected by the surface distribution of phases [21, 22]. As shown in figure 1(d), the FeCoCr-Ag alloys are composed of two phases, i.e. FeCoCr-rich phase surrounded by the network-like Ag-rich phase. This is because Ag has positive heat when mixed with Fe, Co, Cr (Ag–Fe: 28 kJ mol^{-1}; Ag–Co: 19 kJ mol^{-1}; Ag–Cr: 27 kJ mol^{-1}). This large positive heat as a result of mixing leads to grain boundary segregation. The grain size of the FeCoCr-rich phase decreases along with the rise in Ag content. As a consequence, the grain boundary network becomes denser. The increment in area fraction of the Ag-rich phase can be ascribed to increased segregation of Ag at the denser grain boundaries. The widening of Ag phase at grain boundaries is more significant at low amount of Ag addition. At higher Ag content, the widening becomes moderate. The variation tendency of antibacterial ability is consistent with the area fraction of Ag phase. Therefore, the antibacterial ability of the FeCoCr-Ag alloys can be attributed to the release of Ag, which is directly associated with how much Ag phase of the dual-phase structure is exposed to the culture medium.

The variation of the dual-phase structure with Ag content also results in non-monotonic change inhardness. It is reasonable to assume FeCoCr as the hard phase and Ag as the soft phase because the modulus of Ag is lower than that of FeCoCr. The variation of hardness can be understood according to the rule of mixture [23]. As shown in figure 1(d), when the content of Ag is below 20 at.%, the FeCoCr phase dominates the dual-phase structure of the FeCoCr-Ag alloys. Although the increase in Ag content results in an increase in the volume fraction of the soft Ag phase, an accompanying effect is the grain size reduction of the hard FeCoCr phase, which compensates for the Ag-induced softening of the dual-phase structure [24]. As discussed above, when the Ag content is above 20 at.%, the

soft Ag phase dominates the dual-phase structure by forming a denser network. Despite the fact that the grain size of FeCoCr continues to decrease, the strengthening via grain refinement is not enough to compensate for the softening due to the increase in the soft Ag phase, leading to an overall decrease in hardness with an increase in Ag content.

5. Conclusion

In summary, we fabricated alloy libraries out of the FeCoCr-Ag system, which cover a broad composition range (Ag: 4–80 at.%). Through high-throughput characterizations, we revealed the variation of antibacterial ability, mechanical property and adhesion strength with the content of Ag addition. The alloys form a dual-phase structure with the FeCoCr phase embedded in a network-like Ag phase. The optimal Ag content was found to be around 20 at.% at which all of the characterized properties are better than other alloys within the libraries. Our study demonstrates the efficiency of combinatorial methods for the development of high-entropy alloys that combine desired properties.

Acknowledgments

This study was financially supported by the National Natural Science Foundation of China (Grant Nos. 51825104, 12090051 and 12022409), the CAS project (Grant Nos. XDB30000000 and 2022007) and the National Key Research and Development Program of China (Grant No. 2018YFA0703600).

ORCID iD

Yanhui Liu https://orcid.org/0000-0002-7546-3371

References

[1] Yeh J W, Chen S K, Lin S J, Gan J Y, Chin T S, Shun T T, Tsau C H and Chang S Y 2004 Nanostructured high-entropy alloys with multiple principal elements: novel alloy design concepts and outcomes *Adv. Eng. Mater.* **6** 299

[2] Zhang Y, Zuo T T, Tang Z, Gao M C, Dahmen K A, Liaw P K and Lu Z P 2014 Microstructures and properties of high-entropy alloys *Prog. Mater. Sci.* **61** 1

[3] Gludovatz B, Hohenwarter A, Catoor D, Chang E H, George E P and Ritchie R O 2014 A fracture-resistant high-entropy alloy for cryogenic applications *Science* **345** 1153

[4] Wang J, Jiang P, Yuan F and Wu X 2022 Chemical medium-range order in a medium-entropy alloy *Nat. Commun.* **13** 1021

[5] George E P, Raabe D and Ritchie R O 2019 High-entropy alloys *Nat. Rev. Mater.* **4** 515

[6] Zhou E *et al* 2020 A novel Cu-bearing high-entropy alloy with significant antibacterial behavior against corrosive marine biofilms *J. Mater. Sci. Technol.* **46** 201

[7] Ren G *et al* 2022 Enhanced antibacterial behavior of a novel Cu-bearing high-entropy alloy *J. Mater. Sci. Technol.* **117** 158

[8] Gao J, Jin Y, Fan Y, Xu D, Meng L, Wang C, Yu Y, Zhang D and Wang F 2022 Fabricating antibacterial CoCrCuFeNi high-entropy alloy via selective laser melting and *in-situ* alloying *J. Mater. Sci. Technol.* **102** 159

[9] Karlsson H L, Cronholm P, Hedberg Y, Tornberg M, De Battice L, Svedhem S and Wallinder I O 2013 Cell membrane damage and protein interaction induced by copper containing nanoparticles—importance of the metal release process *Toxicology* **313** 59

[10] Hou X, Mao D, Ma H, Ai Y, Zhao X, Deng J, Li D and Liao B 2015 Antibacterial ability of Ag–TiO_2 nanotubes prepared by ion implantation and anodic oxidation *Mater. Lett.* **161** 309

[11] Qin H, Cao H, Zhao Y, Jin G, Cheng M, Wang J, Jiang Y, An Z, Zhang X and Liu X 2015 Antimicrobial and osteogenic properties of silver-ion-implanted stainless steel *ACS Appl. Mater. Interfaces* **7** 10785

[12] Jin G, Qin H, Cao H, Qian S, Zhao Y, Peng X, Zhang X, Liu X and Chu P K 2014 Synergistic effects of dual Zn/Ag ion implantation in osteogenic activity and antibacterial ability of titanium *Biomaterials* **35** 7699

[13] Xia D, Wang X, Wang Y, Wang Y, Meng H, Li L, Zhou P and Xu S 2020 Silver-decorated mesostructured cellular silica foams as excellent antibacterial hemostatic agents for rapid and effective treatment of hemorrhage *Mater. Sci. Eng.* C **115** 111105

[14] Liu Y *et al* 2016 Combinatorial development of antibacterial Zr-Cu-Al-Ag thin film metallic glasses *Sci. Rep.* **6** 26950

[15] Antunes F J, Brito V, Costa H R M, Bastos I N, de Campos J B and de Aguiar R A A 2015 Correlation between chemical composition and adherence of Cr and Co coatings deposited by electric arc *J. Adhes.* **91** 754

[16] Hyslop D J S, Abdelkader A M, Cox A and Fray D J 2010 Electrochemical synthesis of a biomedically important Co–Cr alloy *Acta Mater.* **58** 3124

[17] Comby-Dassonneville S, Venot T, Borroto A, Longin E, der Loughian C, ter Ovanessian B, Leroy M-A, Pierson J-F and Steyer P 2021 ZrCuAg thin-film metallic glasses: toward biostatic durable advanced surfaces *ACS Appl. Mater. Interfaces* **13** 17062

[18] Gao B, Zhou L, Zhang C, Zhu J, Fu L, Yang W and Li D 2021 Effect of microstructural evolution on mechanical and electrical properties of Ag–Mo thin films *Surf. Eng.* **37** 1143

[19] Han L, Jeurgens L P H, Cancellieri C, Wang J, Xu Y, Huang Y, Liu Y and Wang Z 2020 Anomalous texture development induced by grain yielding anisotropy in Ni and Ni-Mo alloys *Acta Mater.* **200** 857

[20] Jabed A, Khan M M, Camiller J, Greenlee-Wacker M, Haider W and Shabib I 2019 Property optimization of Zr-Ti-X (X = Ag, Al) metallic glass via combinatorial development aimed at prospective biomedical application *Surf. Coat. Technol.* **372** 278

[21] Shi A, Zhu C, Fu S, Wang R, Qin G, Chen D and Zhang E 2020 What controls the antibacterial activity of Ti-Ag alloy, Ag ion or Ti_2Ag particles? *Mater. Sci. Eng.* C **109** 110548

[22] Chen M, Zhang E and Zhang L 2016 Microstructure, mechanical properties, bio-corrosion properties and antibacterial properties of Ti–Ag sintered alloys *Mater. Sci. Eng.* C **62** 350

[23] Li F, Liu T, Wang T, Wang A, Wang J and Yang Y 2019 Understanding yielding and the unusual ductile-brittle-ductile transition in Fe-based amorphous nanocrystalline alloy: a combined micromechanical and thermodynamic study *J. Mech. Phys. Solids* **132** 103681

[24] Lu K 2016 Stabilizing nanostructures in metals using grain and twin boundary architectures *Nat. Rev. Mater.* **1** 16019